Hypoplastic interface models for fine-grained soils

H. Stutz[1] and D. Mašín

H. Stutz
Marine and Land Geotechnics / Geomechanics, Institute for Geoscience, Christian Albrechts Universität, Ludewig–Meyn–Str. 10, 24321 Kiel, Germany
Tel.: +49-880-1978
Email:hs@gpi.uni-kiel.de

D. Mašín
Faculty of Science, Charles University in Prague, Albertov 6, 12843 Prague 2, Czech Republic
Email: Masin@natur.cuni.cz

Accepted for publication in *International Journal of Analytical and Numerical Methods in Geomechanics* (11.07.2016)

[1]corresponding author

Abstract

Contact descriptions for interfaces between structural elements (e.g. piles, anchors, tunnel-linings) and soils are widely used in geotechnical engineering. Most of these constitutive interface models, developed for sands, consider 2-D conditions. For clays, only a limited number of 3-D interface models exist. In this paper the fine-grained continuum models based on hypoplastic theories are adapted for the constitutive modelling of fine-grained interfaces. To this end, we develop a general approach to convert the existing continuum soil models into an interface model adopting reduced stress and strain rate vectors and redefining tensorial operations in such a way that the formulation of the existing continuum models can be used without much modification. The Hypoplastic Cam-clay and the explicitly formulated hypoplastic models are adapted to model the interface behaviour. In addition to the reduced stress and strain tensor formulations, we introduce an additional variable reducing the strength and stiffness of the interfaces when compared to the strength and stiffness of the soil. For verification, experiments in constant volume and constant normal stress conditions have been simulated. A comparison of the available experimental data from the literature and the simulations is presented. It is shown that the new hypoplastic interface models can describe a number of important phenomena of clay–structure interfaces.

1. Introduction

Various constitutive models for the contact between soils and structural elements have been proposed in the past. The modelling of interfaces is important for the holistic analysis of geo-structures, such as piles, anchors and retaining walls, where the natural bearing capacity is greatly influenced by the interface zone. The first experimental evidence by Potyondy [1] investigated the effect of various construction materials with different soils, e.g. clay and sands. This research was continued for granular materials and clays, e.g. Tsubakihara et al. [2], Tsubakihara and Kishida [3], Littleton [4], Sun et al. [5]. The experimental research describes the general behaviour of clay interfaces, see [6, 7, 8, 9, 10, 11]. In addition to general interface behaviour, some of the literature describes the rate effect of shearing [12, 13, 14] and the clay interface behaviour at low confining pressures, e.g. [15, 16]. Following this experimental research, the modelling of contact focused on granular–structural interfaces using the elasto-plastic Mohr–Coloumb law, which yields the maximum frictional shear stress in relation to the normal stress. In addition to the classical elasto-plastic models, other formulations have been proposed, for example advanced elasto-plastic models [17, 18], damage models [19, 20], and general plasticity models [21].

The development of interface models for fine-grained soils has evolved as a major development in granular soils. Different models using the disturbed state concept have been proposed explicitly for clay by [6, 22, 23]. Cheng et al. [24] proposed an extension to

the hyperbolic interface model of Clough and Duncan [25], which neglects experimental evidence such as softening behaviour at the interface. Furthermore, there are only a few models formulated as 3-D interface models that can be used in finite element analysis (e.g. Liu et al. [26]). Many of the existing formulations focus on 2-D interface modelling. In addition to the classical elasto-plastic constitutive models, hypoplastic constitutive models have proved to be well suited for modelling the mechanical behaviour of different types of soils. The hypoplastic model proposed by von Wolffersdorf [27] is highly suitable for modelling the 3-D constitutive behaviour of granular materials. This model was reformulated by Gutjahr [28] as a 2-D interface model to simulate retaining wall behaviour. It is based on developments by Herle and Nübel [29], who gave the first hypoplastic granular interface description. These models were extended by Arnold and Herle [30] to a 3-D interface model using a reduced stress and strain tensor, with its underlying formulations from von Wolffersdorf [27]. A potential shortcoming of their approach, which is advanced in this paper, is the consideration of equal normal stresses in all directions in the interface models.
In this paper, we develop a constitutive interface model for fine-grained interfaces on the basis of previous 3-D hypoplastic models. In Mašín [31], a clay hypoplastic model was developed to predict the behaviour of fine-grained soils. The model was subsequently extended to explicitly incorporate asymptotic stress states [32, 33, 34]. The models outlined by Mašín in [32] and [33] have been adapted to model the behaviour of clay–structure interfaces. The models are capable of modelling different surface roughnesses at the structural surface, and they consider different normal stresses that act normally to the interface plane and within the interface plane. The models have been validated by means of constant volume and constant normal stress test simulations. Experimental data from illitic clay [4], Kawasaki clay [3], and a Kaolin clay [5] is used to validate the models.

Notation and conventions

$\|\mathbf{X}\| = \sqrt{\mathbf{X} \cdot \mathbf{X}}$ represents the Euclidean norm of $\mathbf{X}$. The mean effective stress is taken as $p = -\mathrm{tr}\boldsymbol{\sigma}/3$, where the sign convention is from classical continuum mechanics. The stress deviator is represented by $\boldsymbol{\sigma}^* = \boldsymbol{\sigma} + \mathbf{1}p$ and $\mathbf{1}$ denotes the second order unit tensor.

2. Hypoplastic description of clay–structure interfaces

[Figure 1 about here.]

The general form of the hypoplastic model formulation, Gudehus [35], can be written as

$$\dot{\boldsymbol{\sigma}} = f_s \left(\boldsymbol{L} : \dot{\boldsymbol{\varepsilon}} + f_d \boldsymbol{N} \|\dot{\boldsymbol{\varepsilon}}\| \right) \tag{1}$$

where $\dot{\boldsymbol{\sigma}}$ and $\dot{\boldsymbol{\varepsilon}}$ are the stress and strain rate tensors, respectively, $\boldsymbol{N}$ and $\boldsymbol{L}$ are the second and fourth-order constitutive tensors, f_s is the barotropy factor controlling the influence of the mean stress, and f_d is the pyknotropy factor controlling the influence of the relative density. An alternative expression for the hypoplastic model of Mašín [32], developed from the general form of the hypoplastic constitutive formulation in Eq. (1), can be written as

$$\dot{\boldsymbol{\sigma}} = f_s \boldsymbol{L} : \dot{\boldsymbol{\varepsilon}} - \frac{f_d}{f_d^A} \boldsymbol{A} : \boldsymbol{d} \|\dot{\boldsymbol{\varepsilon}}\| \tag{2}$$

where f_d^A describes the value of f_d at the asymptotic state boundary surface (ASBS) and $\boldsymbol{d}$ is the asymptotic strain rate direction. Here, $\boldsymbol{A}$ is

$$\boldsymbol{A} = f_s \boldsymbol{L} + \frac{\boldsymbol{\sigma}}{\lambda^*} \otimes \mathbf{1} \tag{3}$$

where λ^* is a model parameter. Eq. (2) enables the use and incorporation of any appropriate arbitrary shape of the asymptotic shape boundary surface, by specifying the dependence of f_d^A on the void and stress ratio [32]. Eq. (3) is used to further establish the hypoplastic fine-grained interface models. The general underlying assumptions of the strain and stress tensor, proposed by Arnold and Herle [30], are extended in the following sections.

2.1. Interface stress and strain tensor

The novelty of this approach is the consideration of the in-plane stresses and strains. Using the normal stress σ_p, σ_t and shear stresses τ_x and τ_y leads to an identical behaviour of soils under simple shear conditions. Figure 1 illustrates the underlying assumption. Instead of an isotropic stress state [30], a hydrostatic stress state is assumed. In addition, the use of the extended version of the stress and strain vectors leads to the possibility of using any 3-D constitutive model as an interface constitutive model. Under the assumption of a contact plane, where the global axis z is equal to 1 and $2 \| x$ and $3 \| y$ are shown in Figure 1, the stress tensor can be reduced to σ_t, σ_p, $\sigma_{12} = \tau_x$, $\sigma_{13} = \tau_y$. Here σ_t is the transverse stress (normal to the interface), σ_p is the in-plane stress of the interface, and τ_x and τ_y are the shear stress components. The stress tensor is written as

$$\boldsymbol{\sigma}^f = \begin{bmatrix} \sigma_{11} & \sigma_{12} & \sigma_{13} \\ \sigma_{21} & \sigma_{22} & \sigma_{23} \\ \sigma_{31} & \sigma_{32} & \sigma_{33} \end{bmatrix} \Rightarrow \begin{bmatrix} \sigma_t & \tau_x & \tau_y \\ \tau_x & \sigma_p & 0 \\ \tau_y & 0 & \sigma_p \end{bmatrix} \tag{4}$$

where $\boldsymbol{\sigma}^f$ denotes the full stress tensor and the reduced vectorial form $\boldsymbol{\sigma}$ is

$$\boldsymbol{\sigma} = \begin{bmatrix} \sigma_t \\ \sigma_p \\ \tau_x \\ \tau_y \end{bmatrix} \tag{5}$$

[Figure 2 about here.]

We will make a brief comment on the initialization of σ_p: At the beginning of each simulation, which is presented in the following, the stress initialization is done using $\sigma_p = \sigma_t$. After the initialization, the in-plane stress can be developed independently of the normal stress σ_t. Simultaneously, the strain rate tensor $\dot{\boldsymbol{\varepsilon}}$ is defined as

$$\dot{\boldsymbol{\varepsilon}}^f = \begin{bmatrix} \dot{\varepsilon}_{11} & \dot{\varepsilon}_{12} & \dot{\varepsilon}_{13} \\ \dot{\varepsilon}_{21} & \dot{\varepsilon}_{22} & \dot{\varepsilon}_{23} \\ \dot{\varepsilon}_{31} & \dot{\varepsilon}_{32} & \dot{\varepsilon}_{33} \end{bmatrix} \Rightarrow \begin{bmatrix} \dot{\varepsilon}_t & \frac{\dot{\gamma}_x}{2} & \frac{\dot{\gamma}_y}{2} \\ \frac{\dot{\gamma}_x}{2} & 0 & 0 \\ \frac{\dot{\gamma}_y}{2} & 0 & 0 \end{bmatrix} \tag{6}$$

where $\dot{\boldsymbol{\varepsilon}}^f$ denotes the full strain rate tensor, $\dot{\epsilon}_t$ the normal strain rate, and $\frac{\dot{\gamma}_x}{2}; \frac{\dot{\gamma}_y}{2}$ the shear strain rates in the x and y directions. The reduced vectorial form $\dot{\boldsymbol{\varepsilon}}$ is defined as

$$\dot{\boldsymbol{\varepsilon}} = \begin{bmatrix} \dot{\varepsilon}_t \\ 0 \\ \frac{\dot{\gamma}_x}{2} \\ \frac{\dot{\gamma}_y}{2} \end{bmatrix} \tag{7}$$

Notice that the in-plane component of the strain rate tensor is always assumed to be zero.

2.2. Shear zone thickness

As introduced by Gutjahr [28], the shear strain γ_i is connected to the interface displacement u_i by the shear zone thickness. This thickness d_s for clay interfaces is analogous to granular materials. Because of the relation between the soil type and the surface roughness (Figure 2), γ_i can be written as

$$\tan \gamma_i = \frac{u_i}{d_s} \tag{8}$$

where d_s is the shear zone thickness, which is influenced by the clay mineralogy and the surface roughness. The experimental evidence of the shear zone thickness for clays was studied by Lupini et al. [9] using a ring-shear test apparatus. Chen et al. [7] stated that the shear zone thickness is $7-8$ times the mean diameter d_{50}. However, the shear-band thickness at the interface zone is difficult to examine. For this reason, d_s can be obtained from back calculations, as suggested by Arnold and Herle [30].

2.3. General definitions of some new operators

Our modelling approach was introduced in Stutz et al. [36]. By retaining the continuum constitutive models, the redefined tensorial operators in combination with the reduced stress Eq. (5) and strain rate vectors Eq. (7) are used to simulate the interface behaviour. By employing this approach, the results coincide with the modelling of simple shear

conditions using the full 3-D continuum models.
The Voigt notation is used to reduce the second order and fourth order tensors to vectors and matrices. The first rank tensors $\boldsymbol{X}$ and $\boldsymbol{Y}$ and the second rank tensor $\mathcal{S}$ are defined as

$$\boldsymbol{X} = \begin{bmatrix} X_1 \\ X_2 \\ X_3 \\ X_4 \end{bmatrix} \quad \boldsymbol{Y} = \begin{bmatrix} Y_1 \\ Y_2 \\ Y_3 \\ Y_4 \end{bmatrix} \quad \mathcal{S} = \begin{bmatrix} S_{11} & S_{12} & S_{13} & S_{14} \\ S_{21} & S_{22} & S_{23} & S_{24} \\ S_{31} & S_{32} & S_{33} & S_{34} \\ S_{41} & S_{42} & S_{43} & S_{44} \end{bmatrix} \tag{9}$$

The Euclidean norm of $\boldsymbol{X}$ is then written as

$$\|\boldsymbol{X}\| = \sqrt{X_1^2 + 2X_2^2 + 2X_3^2 + 2X_4^2} \tag{10}$$

The trace of $\boldsymbol{X}$ is defined as

$$tr\left(\boldsymbol{X}\right) = X_1 + 2X_2 \tag{11}$$

The determinant of $\boldsymbol{X}$ is defined as

$$\det\left(\boldsymbol{X}\right) = \mathbf{1} : \boldsymbol{X} = X_1 X_2^2 - X_4^2 X_2 - X_3^2 X_2 \tag{12}$$

The second-order unit tensor used in the vectorial notation is

$$\mathbf{1} = \begin{bmatrix} 1 \\ 1 \\ 0 \\ 0 \end{bmatrix} \tag{13}$$

The fourth order unit tensor is

$$\boldsymbol{I} = \begin{bmatrix} 1 & 0 & 0 & 0 \\ 0 & 0.5 & 0 & 0 \\ 0 & 0 & 0.5 & 0 \\ 0 & 0 & 0 & 0.5 \end{bmatrix} \tag{14}$$

The deviator $\boldsymbol{X}^*$ is written as

$$\boldsymbol{X}^* = \boldsymbol{X} + \mathbf{1}\left(\frac{-tr\boldsymbol{X}}{3}\right) = \begin{bmatrix} \frac{2}{3}X_1 - \frac{2}{3}X_2 \\ \frac{X_2}{3} - \frac{X_1}{3} \\ X_3 \\ X_4 \end{bmatrix} \tag{15}$$

The normalized deviator $\hat{\boldsymbol{X}}^*$ is defined in vectorial notation as

$$\hat{\boldsymbol{X}}^* = \frac{\boldsymbol{X}}{tr\boldsymbol{X}} - \frac{\boldsymbol{1}}{3} = \begin{bmatrix} \frac{X_1}{X_1+2X_2} - \frac{1}{3} \\ \frac{X_2}{X_1+2X_2} - \frac{1}{3} \\ \frac{X_3}{X_1+2X_2} \\ \frac{X_4}{X_1+2X_2} \end{bmatrix} \tag{16}$$

The inner product $(\cdot)$ is

$$\boldsymbol{X} \cdot \boldsymbol{Y} = \begin{bmatrix} X_1Y_1 + X_3Y_3 + X_4Y_4 \\ X_2Y_2 + X_3Y_3 \\ X_1Y_3 + X_3Y_2 \\ X_4Y_1 + X_2Y_4 \end{bmatrix} \tag{17}$$

The double inner product (:) between the two first-rank tensors is defined as

$$\boldsymbol{X} : \boldsymbol{Y} = X_1Y_1 + 2X_2Y_2 + 2X_3Y_3 + 2X_4Y_4 \tag{18}$$

The double inner product (:) between second-rank and first-rank tensors is defined as

$$\mathcal{S} : \boldsymbol{Y} = \begin{bmatrix} S_{11}Y_1 + 2S_{12}Y_2 + 2S_{13}Y_3 + 2S_{14}Y_4 \\ S_{21}Y_1 + 2S_{22}Y_2 + 2S_{23}Y_3 + 2S_{24}Y_4 \\ S_{31}Y_1 + 2S_{32}Y_2 + 2S_{33}Y_3 + 2S_{34}Y_4 \\ S_{41}Y_1 + 2S_{42}Y_2 + 2S_{43}Y_3 + 2S_{44}Y_4 \end{bmatrix} \tag{19}$$

Furthermore, the outer product $(\otimes)$ is defined as

$$\boldsymbol{X} \otimes \boldsymbol{Y} = \begin{bmatrix} X_1Y_1 & X_1Y_2 & X_1Y_3 & X_1Y_4 \\ X_2Y_1 & X_2Y_2 & X_2Y_3 & X_2Y_4 \\ X_3Y_1 & X_3Y_2 & X_3Y_3 & X_3Y_4 \\ X_4Y_1 & X_4Y_2 & X_4Y_3 & X_4Y_4 \end{bmatrix} \tag{20}$$

These definitions are used in the following sections, where only the standard tensorial notation is given for the contact models. As an example, the reduced vectorial formulation of the Hypoplastic Cam-clay model is given in Appendix A.

2.4. Hypoplastic Cam-clay interface model

The hypoplastic Cam-clay model [32] is introduced briefly. Using the reduced stress tensor Eq. (5) and the reduced strain tensor Eq. (7) from the main model, the hypoplastic

Cam-clay interface model (HCC) can be reformulated as

$$\dot{\boldsymbol{\sigma}} = f_s \boldsymbol{L} : \dot{\boldsymbol{\varepsilon}} - \left(\frac{p}{p_e^*}\right) \frac{M^2 + \eta^2}{M^2} \left(f_s \boldsymbol{L} + \frac{\boldsymbol{\sigma}}{\lambda^*} \otimes \mathbf{1}\right) : \boldsymbol{d} \|\dot{\boldsymbol{\varepsilon}}\| \tag{21}$$

where M is the slope of the critical state line in the p–q plane.The stress ratio is $\eta = \frac{q}{p}$ and the deviatoric invariant is defined as $q = \sqrt{\frac{3}{2}} \|\boldsymbol{\sigma}^*\|$. The $\boldsymbol{L}$ tensor, representing the isotropic elasticity, is given by

$$\boldsymbol{L} = \boldsymbol{I} + \frac{\nu}{1 - 2\nu} \mathbf{1} \otimes \mathbf{1} \tag{22}$$

where ν controls the ratio between the shear and the bulk stiffnesses. The Hvorslev equivalent pressure p_e^* is defined as

$$p_e^* = p_r \exp\left[\frac{N - \ln(1 + e)}{\lambda^*}\right] \tag{23}$$

where p_r is the reference stress of 1 kPa, e is the void ratio, and N and λ^* are model parameters. The asymptotic strain rate direction $\boldsymbol{d}$ is assumed to be normal to the ASBS, following the modified Cam-clay formulation. The asymptotic strain rate direction $\boldsymbol{d}$ can thus be written as

$$\boldsymbol{d} = \frac{3\boldsymbol{\sigma}^* - \mathbf{1} p \frac{M^2 - \eta^2}{3}}{\|3\boldsymbol{\sigma}^* - \mathbf{1} p \frac{M^2 - \eta^2}{3}\|} \tag{24}$$

The barotropy factor f_s is calculated using

$$f_s = \frac{3p}{2} \left(\frac{1}{\lambda^*} + \frac{1}{\kappa^*}\right) \frac{1 - 2\nu}{1 + \nu} \tag{25}$$

We make use of the reduced stress Eq. (5) and strain vectors Eq. (7) in combination with the above reduced new tensor operators (Section 2.3) to define the hypoplastic Cam-clay model as given in the Appendix A. The hypoplastic Cam-clay model uses the same parameters as the modified Cam-clay model, where the slope of the critical state line M is calculated using the critical state friction angle:

$$M = \frac{6 \sin \phi_c}{3 - \sin \phi_c} \tag{26}$$

The parameter λ^* is the slope of the isotropic normal compression line in $\ln(1+e)$ versus $\ln(p)$ and κ^* controls the unloading line in the same plane, N is the value of $\ln(1 + e)$ at the isotropic normal compression line for $p = p_r = 1$ kPa, and ν controls the shear stiffness. In addition, the void ratio e and $\boldsymbol{\sigma}$ are used as state variables.

2.5. Clay hypoplasticity interface model with advanced asymptotic state boundary surface

Based on the clay hypoplasticity model given in [31] with explicitly defined asymptotic states [33], the corresponding interface model is derived by using the reduced stress and strain tensors, as shown in Eq. (5) and Eq. (7). The model uses the general formulation of hypoplasticity with explicitly defined asymptotic states in Eq. (2). There are some differences from the hypoplastic Cam-clay model in [32], which are presented below. The constitutive tensors $\boldsymbol{L}$, f_s and $\boldsymbol{A}$ are the same as those in the model presented in Section 2.4, and f_d is proposed in [33] as

$$f_d = \left(\frac{2p}{p_e}\right)^{\alpha_f} \tag{27}$$

The exponent α_f controls the irreversible deformation inside the ASBS. In [34], Mašín suggests the use of α_f from [31], which leads to a better prediction of the model response. Additionally, α_f can be treated as an independent parameter [31] to control the non-linear response inside the ASBS.

$$\alpha_f = \frac{ln\left(\dfrac{\lambda^* - \kappa^*}{\lambda^* + \kappa^*}\left(\dfrac{3 + a_f^2}{a_f\sqrt{3}}\right)\right)}{ln\,(2)} \tag{28}$$

where a_f is

$$a_f = \frac{\sqrt{3}\,(3 - \sin\phi_c)}{2\sqrt{2}\sin\phi_c} \tag{29}$$

The factor f_d^A is the limiting value of f_d at the ASBS, i.e.

$$f_d^A = 2^{\alpha_f}\,(1 - F_m)^{\alpha_f/\omega} \tag{30}$$

The Matsuoka–Nakai factor F_m [37] is calculated by

$$F_m = \frac{9I_3 + I_1 I_2}{I_3 + I_1 I_2} \tag{31}$$

using the following invariants:

$$I_1 = tr\boldsymbol{\sigma} \qquad I_2 = \frac{1}{2}\left[\boldsymbol{\sigma} : \boldsymbol{\sigma} - (I_1)^2\right] \qquad I_3 = \det\boldsymbol{\sigma} \tag{32}$$

$$\omega = -\frac{ln\left(\cos^2\phi_c\right)}{ln\,(2)} + a_f\left(F_m - \sin^2\phi_c\right) \tag{33}$$

with the Lode angle θ,

$$\cos 3\theta = -\sqrt{6}\frac{tr\left(\hat{\boldsymbol{\sigma}}^* \cdot \hat{\boldsymbol{\sigma}}^* \cdot \hat{\boldsymbol{\sigma}}^*\right)}{\left[\hat{\boldsymbol{\sigma}}^* : \hat{\boldsymbol{\sigma}}^*\right]^{3/2}} \tag{34}$$

The asymptotic strain rate direction $\boldsymbol{d}$ is given by

$$\boldsymbol{d} = \frac{\boldsymbol{d}^A}{\|\boldsymbol{d}^A\|} \tag{35}$$

where $\boldsymbol{d}^A$ is

$$\boldsymbol{d}^A = -\hat{\boldsymbol{\sigma}}^* + \mathbf{1}\left[\frac{2}{3} - \frac{1}{4}F_m^{1/4}\right]\frac{F_m^{\xi/2} - \sin^\xi \phi_c}{1 - \sin^\xi \phi_c} \tag{36}$$

The factor ξ controls the ratio of the volumetric strain to the shear strain: this factor was obtained using an optimisation procedure to ensure that the strain rate direction satisfies approximately the Jaky formula [38]:

$$\xi = 1.7 + 3.9 \sin^2 \phi_c \tag{37}$$

The combination of all components of the clay hypoplastic model with explicitly defined asymptotic states (see Eq. (2)) leads to the interface model (HCE) using the newly defined tensor operators given in Section 2.3.
The model requires 5 parameters: ϕ_c the critical state friction angle, λ^*, κ^*, N and ν (see Section 2.4).
Note that in finite element codes, the models for interfaces are typically implemented with the primary state variables, the stress and strain rate normal to the interface (σ_t, $\dot{\varepsilon}_p$), and shear components (τ_x,τ_y,$\dot{\gamma}_x$,$\dot{\gamma}_y$). To incorporate the in-plane stress into the formulation, σ_p must be considered as an additional state variable along with the void ratio e.

2.6. Extension by surface roughness

One of the key factors for modelling the soil–structure interface is the roughness, as shown in [1], [4], and [5]. The approach suggested by [30] is used to incorporate the surface roughness into the HCC and HCE models, where κ_r is the friction coefficient, which can be calculated depending on the surface traction profile of the structural element that is in contact with the surrounding soil. If the surface condition is not completely rough, the frictional coefficient $\phi_{interface} \leq \phi_c$, and the value of κ_r is

$$\kappa_r = \frac{\phi_{interface}}{\phi_c} \tag{38}$$

The introduction of κ_r into the HCC model is done by modification of the parameter M for the critical state line:

$$M = \frac{6\sin(\phi_c \kappa_r)}{3 - \sin(\phi_c \kappa_r)} \tag{39}$$

Additionally, Arnold and Herle [30] suggested a reduction of the barotropy factor f_s of the hypoplastic model to decrease the predicted soil stiffness. This modifies the model response both in compression and in shear. In our model, we assume that it is more realistic to reduce the response in shear only. We adopt the formulation originally

proposed in [39], and later adopted in Mašín [31]. The shear stiffness is governed by the variable r. In clay hypoplasticity, the value of r is equal to (see Mašín [33])

$$r = \frac{4}{3}\frac{\kappa^*}{\lambda^* + \kappa^*}\frac{1+\nu}{1-2\nu} \tag{40}$$

The value of r for the reduced shear stiffness (denoted by r_r) is

$$r_r = \frac{4/\kappa_r}{3}\frac{\kappa^*}{\lambda^* + \kappa^*}\frac{1+\nu}{1-2\nu} \tag{41}$$

and the value of ν_r used in the modified model in place of ν is

$$\nu_r = \frac{3r_r\left(\lambda^* + \kappa^*\right) - 4\kappa^*}{6r_r\left(\lambda^* + \kappa^*\right) + 4\kappa^*} \tag{42}$$

In the HCE model, the same equations are adopted for the implementation of the structural surface roughness. In addition, a_f is modified:

$$a_f = \frac{\sqrt{3}\left(3 - \sin\phi_c\kappa_r\right)}{2\sqrt{2}\sin\phi_c\kappa_r} \tag{43}$$

ω, adopted for the surface roughness extension, is

$$\omega = -\frac{ln\left(\cos^2\phi_c\kappa_r\right)}{ln\left(2\right)} + a_f\left(F_m - \sin^2\phi_c\kappa_r\right) \tag{44}$$

and $\boldsymbol{d}^A$, used for the calculation of the asymptotic strain rate direction, becomes

$$\boldsymbol{d}^A = -\hat{\boldsymbol{\sigma}}^* + \mathbf{1}\left[\frac{2}{3} - \frac{1}{4}F_m^{1/4}\right]\frac{F_m^{\xi/2} - \sin^\xi\phi_c\kappa_r}{1 - \sin^\xi\phi_c\kappa_r} \tag{45}$$

3. General model behaviour

The two different hypoplastic fine-grained interface models are used both for constant volume (undrained) and constant normal stress boundary conditions simulations. The parameters for the calculations are given in Table 1. These are artificial parameters used by Mašín in [32, 33]. The HCC model uses the parameter M calculated from Eq. (39)

[Table 1 about here.]

for mutual comparability. K is introduced as

$$K = \dot{\sigma}_t/\dot{\varepsilon}_t \tag{46}$$

Typically, experiments are described as follows [40].

- Constant Volume (CV):

$K = \infty$; $\dot{\sigma}_t \neq 0$; $\dot{\varepsilon}_t = 0$, see Section 3.1

- Constant Normal Stress (CNL):
  $K = 0$; $\dot{\sigma}_t = 0$; $\dot{\varepsilon}_t \neq 0$, see Section 3.2

[Figure 3 about here.]

3.1. Constant volume calculations

[Figure 4 about here.]

The parameters from Table 1 were used for the calculation of the interface models under CV-conditions. The CV-test conditions, compared to conventional 3-D soil testing conditions (triaxial testing), often refer to undrained behaviour ($\dot{\varepsilon}_t = 0$) of the interface. In addition, $\dot{\varepsilon}_t = 0$ implies a constant void ratio $\dot{e} = 0$.
The simulations were done under two different normal stress conditions (100 and 300

[Figure 5 about here.]

kPa). Figure 4 shows the shear stress τ_x vs shear strain γ_x results, Figure 5 shows the normal stress σ_t vs shear strain γ_x results, and Figure 6 shows the normal stress σ_t vs shear strain τ_x path of the interface. Clearly, the HCE model predicts lower final shear stresses than the HCC model, although both models were calibrated to have the same critical state friction angle. The reason for this difference is the more advanced shape of the ASBS of the HCE model with a Matsuoka–Nakai deviatoric cross-section. The HCE model predicts lower critical state stress ratios because the Lode angles in the shear tests are different from the Lode angles associated with triaxial compression tests.
In general the observed behaviour is typically associated with undrained (constant volume) conditions, as shown in the results of experimental research presented in Tsubakihara and Kishida [3] and Sun et al. [5].

[Figure 6 about here.]

3.2. Constant normal stress calculations

[Figure 7 about here.]

The next section deals with simple shear conditions. From Figure 1, it can be seen that the shear conditions are the same as the simple shear conditions in a soil continuum. This test condition is highlighted as constant normal stress ($\dot{\sigma}_t = 0$) and a change in normal deformation to the interface ($\dot{\varepsilon}_t \neq 0$). The results of these calculations are shown

in Figures 7 and 8.
Figure 7 shows the shear deformation γ_x vs shear stress τ_x behaviour. It can be seen that both models have the same trend but differ in the residual shear stress: both models have a similar stress path at small shear deformations.
A similar behaviour can be observed in Figure 8. At higher pressures (300 [kPa]), the

[Figure 8 about here.]

behaviour of the normal strain $\dot{\varepsilon}_t$ vs the shear strain γ_x tends to be identical; however, the models behave differently from each other at lower pressures (100 kPa). The normal strain rate in the HCE model is higher than with the HCC model.
Figure 9 presents the effect of the applied initial normal stress condition. The approach proposed by Stutz et al. [36], which is used in this paper, is compared to the approach proposed by Arnold and Herle [30]. In addition, an initial stress condition is used by assuming $K_0 = 0.5$. The results show that the use of an isotropic stress condition [30] leads to a smaller peak stress than the hydrostatic stress assumption [36], while using an initial applied stress of $\sigma_p = K_0 * \sigma_0$ leads to a softer model response. Considering a simple shear simulation, as shown in Figure 3, the assumption of initial hydrostatic stress conditions leads to the same results as the full 3-D constitutive hypoplastic model.

[Figure 9 about here.]

3.3. Simulations using the surface roughness extension

[Figure 10 about here.]

In Section 2.6, the explicit modelling of the surface roughness was introduced. This development is studied in the following. Here, $\kappa_r \leq 1$ should tend to a soft response at the interface rather than using the full rough conditions with $\kappa_r = 1.0$. The surface roughness extension for both models has been examined using different κ_r and the parameters from Table 1.
The three different κ_r values used are 1.0, 0.75 and 0.5; the results for the τ_x vs γ_x simulations are shown in Figure 10. In both models, there is a softer response for $\kappa_r < 1.0$. The surface extensions for the HCC and HCE models are able to incorporate the effect of the surface roughness, as expected.

4. Model validation using experimental data

[Table 2 about here.]

In this section, the ability to model different clay interfaces is shown for the Hypoplastic Cam-clay (HCC) and extended Hypoplastic (HCE) models. The experimental data

from Littleton [4] and Tsubakihara et al. [2, 3] is used to validate the HCC and HCE models under constant normal load. In addition, newer data available from Sun et al. [5] was used for the comparison of experimental to simulation results under constant volume conditions.
The parameters used are given in Table 2 while the properties of the clays are summarized in Table 3: only the common physical properties are given, which are readily available in the literature and described in the papers cited. For the clays used in this

[Table 3 about here.]

section, the hypoplastic parameters were not available. Therefore the parameters used for the verification were estimated by a simple trial and error procedure. In order to make a reasonable comparison between the HCE and HCC models, the parameters used in the calculations must be the same. Those used in Sections 4.1 and 4.3 are the same. However, in Section 4.2, different parameters were used, to demonstrate the capabilities of the models.

4.1. Simulations of the experimental data from Littleton [4]

Littleton [4] conducted tests on two different clays, using a modified direct shear test. The lower part of the box was replaced by a solid mild steel block. The average roughness was 0.18 μm in the centre line of the block, with a cut-off length of 0.84 mm. The shear box was used in both a modified and a conventional manner, to find the internal (soil–soil) and external (soil–solid) frictional shear strengths [4]. The two materials used by Littleton [4] were Kaolin clay and an illitic clay. The results from the illitic clay

[Figure 11 about here.]

were used for the verification. The illitic clay was mixed to a moisture content of 90%. The clay was consolidated under a gradually increasing load, to ensure that 95% of the consolidation had taken place. The properties of the clay are given in Table 3. The parameters used for the verification are given in Table 2. The vertical load of the test was 626 N. The behaviour of the illitic clay and the solid mild steel block shows the typical behaviour of clay interfaces, with a higher peak at smaller displacements and lower residual shear strength at larger displacements compared to soil–soil direct shear tests. Figure 11 shows the result in a tangential displacement u_x vs shear stress τ_x graph. The experimental behaviour was simulated using both the HCC and HCE models in a quantitative manner, with the HCC model showing a higher peak shear stress than the HCE model. The reason for this unexpected behaviour is the use of one parameter set for both models: we had anticipated that one hypoplastic parameter set would be satisfactory to validate both models, but clearly the simulations using the HCC model can be improved by using a different set of parameters.
In summary, both the HCC and HCE models were, after a calibration, able to simulate the interface behaviour of illitic clay.

4.2. Simulations of the experimental data from Kawasaki clay [2, 3]

[Figure 12 about here.]

Tsubakihara and Kishida [2] used both simple and direct shear devices for constant normal stress tests of Kawasaki clay to study the effect of surface roughness and the different test devices to determine how they influenced the interface frictional behaviour. The soils used were reconstituted Kawasaki marine clay (S0) and Kawasaki marine clay mixed with Toyoura sand (S4) (see Table 3). The samples were consolidated at 294.4 kPa, respectively, 98 kPa. After the application of a vertical consolidation pressure, the stress was held constant during the test (constant normal stress condition).
Low-carbon steel was used as the construction material in the apparatus and the surface roughness was investigated and measured. The experimental data used as comparison for the HCE and HCC models was from the simple shear testing device under constant pressure (CNL conditions) [3].
In the following, we used different parameters sets in the HCE and HCC models to demonstrate the simulation capability. The different model parameter sets are given in Table 3. The roughness coefficients used in both models are $\kappa_r = 1.0$ for 10μm and $\kappa_r = 0.95$ for 3μm at a constant normal load of 294 kPa. For the calculation at a constant normal load of 98 kPa, κ_r is taken to be 0.85. Figure 12 shows the results, for the

[Figure 13 about here.]

verification data using the Kawasaki clay (S0), in the form of a shear strain γ_x vs shear stress τ_x diagram for the HCE model. There is a good match between the experimental data and the simulation results for all normal loads and different roughness values. The results of the HCC model, illustrated in Figure 13, show the same results, although the simulations show a over-prediction compared to the experimental data. Both the HCC and HCE models are able to reproduce the behaviour of the experimental data reported by [2, 3].
Both models were used to simulate the experimental results for a mixture of Kawasaki clay and Toyoura sand (S4): these results are shown in Figure 14. The applied constant load in this test by Tsubakihara et al. [2] was 294 kPa. As already mentioned, the HCC and HCE models can simulate the experimental result with good agreement.

[Figure 14 about here.]

4.3. Clay-Interface undrained shear tests from [5]

Sun et al. [5] conducted tests using a modified direct shear apparatus under constant volume conditions with different mixtures of clay and sand, and varying the roughness of the steel plates. The data for pure Kaolin clay is used for verification. This clay was tested under normally consolidated conditions at a consolidation pressure of 98 kPa and low-carbon steel was used as the structural surface.

The effect of the consolidation ratio, surface roughness, and shearing rate, was recorded by Sun et al. [5]. The consolidation pressure was 400 kPa in the experimental data and the shearing rate 1 mm/min. This shearing rate is the lowest applied by Sun et al. [5].

Figure 15 gives the result as a plot of the shear displacement u_x vs the shear stress

[Figure 15 about here.]

τ_x. There is no good agreement between the simulation and experimental results for the peak stress. In addition, the general stress paths differ at higher deformations. Nevertheless, both the HCE and HCC models can be used to model the behaviour from constant volume test conditions at interfaces, as demonstrated in Section 3.1.

5. Concluding remarks

In this paper, we have used a general approach [36] to convert existing continuum soil models into interface models. In this approach, reduced stress and strain rate vectors and re-defined tensorial operations are adopted in order to use the formulation of the existing continuum models without significant modification. Based on this approach, we have proposed interface versions of two clay hypoplastic models: the hypoplastic Cam-clay model and the more advanced clay hypoplastic model with an explicit state boundary surface formulation. In addition to the reduced stress and strain vector formulation, a parameter is introduced that decreases the interface strength and interface shear stiffness when compared to the corresponding continuum model, so as to account for the surface roughness at the interface.

In the second part of the paper, the general response of each model was shown and the differences between the predictions obtained using the two models were discussed. Finally, the models were evaluated with respect to the existing experimental data. This evaluation was limited, due to the scant experimental database available in the literature. Additional evaluation is planned for future work.

The modelling of an interface by applying 3-D constitutive models was achieved by using 3-D constitutive soil models. This is in accordance with Arnold [41], who highlighted the fact that interface behaviour is similar to soil behaviour. On the other hand, using the approach of Weißenfels and Wriggers [42, 43], the models reformulated in this paper can be implemented in standard finite element simulations. The proposed constitutive interface models can be used in zero-thickness interface elements [44, 45] or mortar methods, e.g. [46].

Lastly, there are further possibilities for using the modified tensorial notation: with some modifications for the surface roughness, this method can be applied to various constitutive models. For example, the hypoplastic model by Von Wolffersdorff [27] is used by Stutz et al. [36] for modelling interface behaviour. This scheme can used for elasto-plastic models as well as for hypoplastic models. The main thing is to modify the surface roughness approach.

Acknowlegdement

The first author greatly appreciates financial support by the German Research Foundation in the framework of research training group 1462. The second author greatly appreciates financial support by research grant 15-05935S of the Czech Science Foundation.

References

[1] Potyondy JG. Skin friction between various soils and construction materials. *Géotechnique* 1961; **11**:339–353.

[2] Tsubakihara Y, Kishida H, Nishyama T. Friction between cohesive soils and steel. *Soils and Foundations* 1993; **33**(2):145–156.

[3] Tsubakihara Y, Kishida H. Frictional behaviour between normally consolidated clay and steel by two direct shear type apparatuses. *Soils and Foundations* 1993; **33**(2):1–13.

[4] Littleton I. An experimental study of the adhesion between clay and steel. *Journal of Terramechanics* 1976; **13**(3):141–152.

[5] Sun D, Matsuoka H, Morichi K, Tanaka Y, Yamamoto H. Frictional behaviour between clay and steel by two direct shear type apparatus. *Deformation Charateristics of Geomaterials*, 2003; 239–245.

[6] Desai C, Rigby D. Cyclic interface and joint shear device including pore pressure effects. *Journal of Geotechnical and Geoenvironmental Engineering* 1997; **123**(6):568–579.

[7] Chen X, Zhang J, Xiao Y, Li J. Effect of roughness on shear behavior of red clay-concrete interface in large-scale direct shear tests. *Canadian Geotechnical Journal* Jan 2015; **52**:1122–1135.

[8] Lemos LJL, Vaughan PR. Clay–Interface shear resistance. *Géotechnique* 2000; **50**(1):55–64.

[9] Lupini F, Skinner AE, Vaughan PR. The drained residual strength of cohesive soils. *Géotechnique* 1981; **31**(2):181–213.

[10] Ovando-Shelley E. Direct shear tests on Mexico City clay with reference to friction pile behaviour. *Geotechnical and Geological Engineering* 1995; **13**:1–16.

[11] Taha A, Fall M. Shear behavior of sensitive marine clay–steel interfaces. *Acta Geotechnica* 2014; :969–980.

[12] Jardine RJ, Lehane BM. Residual strength characteristics of Bothkennar clay. *Géotechnique* 1992; **42**(2):363–367.

[13] Tika-Vassolokos T. Clay-on-steel ring shear tests and their implications for displacement piles. *Geotechnical Testing Journal* 1991; **14**(4):457–463.

[14] Vaughan PR, Lemos LJLJ, Tika TE. Fast shearing of pre-existing shear zones in soil. *Géotechnique* 1996; **46**(2):197–233.

[15] Eid HT, Amarasinghe RS, Rabie KH, Wijewickreme D. Residual shear strength of fine-grained soils and soil-solid interfaces at low effective normal stresses. *Canadian Geotechnical Journal* 2014; **13**(January):1–13.

[16] Najjar SS, Gilbert RB, Liedtke E, McCarron B, Young A. Residual shear strength for interfaces between pipelines and clays at low effective normal stresses. *Journal of Geotechnical and Geoenvironmental Engineering* 2007; **133**(6):695–706.

[17] Ghionna VN, Mortara G. An elastoplastic model for sand–structure interface behaviour. *Géotechnique* 2002; **52**(1):41–50.

[18] Lashkari A. Prediction of the shaft resistance of nondisplacement piles in sand. *International Journal for Numerical and Analytical Methods in Geomechanics* 2013; :904–931.

[19] Hu L, Pu JL. Application of damage model for soil-structure interface. *Computers and Geotechnics* Mar 2003; **30**(2):165–183.

[20] Zhang G, Zhang J. State of the art: Mechanical behavior of soil–structure interface. *Progress in Natural Science* Oct 2009; **19**(10):1187–1196.

[21] Liu H, Song E, Ling HI. Constitutive modeling of soil–structure interface through the concept of critical state soil mechanics. *Mechanics Research Communications* 2006; **33**(4):515–531.

[22] Samtani NC, Desai CS, Vulliet L. An interface model to describe viscoplastic behavior. *International Journal for Numerical and Analytical Methods in Geomechanics* 1996; **20**(March 1995):231–252.

[23] Shao RC, Desai CS. Implementation of DSC model and application for analysis of field pile tests under cyclic loading. *International Journal for Numerical and Analytical Methods in Geomechanics* 2000; **24**:601–624.

[24] Cheng Z, Chunfeng Z, Hui G. Elastoplastical analysis of the interface between clay and concrete incorporating the effect of the normal stress history. *Journal of Applied Mathematics* 2013; **2013**:1–12.

[25] Clough GW, Duncan JM. Finite element analyses of retaining wall behaviour. *Journal of Soil Mechanics and Foundation Division* 1971; (12):1657–1673.

[26] Liu J, Zou D, Kong X. A three-dimensional state-dependent model of soil-structure interface for monotonic and cyclic loadings. *Computers and Geotechnics* 2014; **61**:166–177.

[27] von Wolffersdorff PA. Hypoplastic relation for granular materials with a predefined limit state surface. *Mechanics of Cohesive-Frictional Materials* 1996; **1**(3):251–271.

[28] Gutjahr S. Optimierte Berechnung von nicht gestützten Baugrubenwänden in Sand. Heft 25, TU Dortmund 2003.

[29] Herle I, Nübel K. Hypoplastic description of interface behaviour. *Numerical Models in Geomechanics–NUMOG VII*, Pande G, Pietruszczak S, Schweiger H (eds.), 1999.

[30] Arnold M, Herle I. Hypoplastic description of the frictional behaviour of contacts. *Numerical Methods in Geotechnical Engineering*, Schweiger H (ed.), 2006; 101–106.

[31] Mašín D. A hypoplastic constitutive model for clays. *International Journal for Numerical and Analytical Methods in Geomechanics* 2005; **29**:311–336.

[32] Mašín D. Hypoplastic Cam-clay model. *Géotechnique* 2012; **62**(6):549–553.

[33] Mašín D. Clay hypoplasticity with explicitly defined asymptotic states. *Acta Geotechnica* 2013; **8**:481–496.

[34] Mašín D. Clay hypoplasticity model including stiffness anisotropy. *Géotechnique* 2014; **2**(3):232–238.

[35] Gudehus G. A comprehensive constitutive equation for granular materials. *Soils and Foundations* 1996; **36**(1):1–12.

[36] Stutz H, Mašín D, Wuttke F. Enhancement of a hypoplastic model for granular soil–structure interface behaviour. *Acta Geotechnica* 2016; :1–13doi:10.1007/s11440-016-0440-1.

[37] Matsuoka H, Nakai T. Stress-deformation and strength characteristics of soil under three different principal stresses. *Proceedings of the Japanese Society of Civil Engineers, vol 232*, 1974; 59–70.

[38] Jaky J. Pressure in silos. *2nd ICSMFE*, 1948; 103–107.

[39] Herle I, Kolymbas D. Hypoplasticity for soils with low friction angles. *Computers and Geotechnics* Jul 2004; **31**(5):365–373.

[40] Evgin E, Fakharian K. Effect of stress paths on the behaviour of sand-steel interfaces. *Canadian Geotechnical Journal* 1996; **33**:853–865.

[41] Arnold M. Application of the intergranular strain concept to the hypoplastic modelling of non-adhesive interfaces. *The 12th International Conference of International Association for Computer Methods and Advances in Geomechanics (IACMAG)*, 2008; 747–754.

[42] Weißenfels C, Wriggers P. A contact layer element for large deformations. *Computational Mechanics* 2015; **55**(5):873–885.

[43] Weißenfels C, Wriggers P. Methods to project plasticity models onto the contact surface applied to soil structure interactions. *Computers and Geotechnics* 2015; **65**:187–198.

[44] Goodman RE, Taylor RL, Brekke TL. A model for the mechanics of jointed rock. *Journal of the Soil mechanics and Foundations Division* 1968; **94**:637–657.

[45] Beer G. An isoparametric joint/interface element for finite element analysis. *International Journal for Numerical and Analytical Methods in Geomechanics* 1985; **21**:585–600.

[46] Belgacem F, Hild P, Laborde P. The mortar finite element method for contact problems. *Mathematical and Computer Modelling* 1998; **28**(4-8):263–271.

A. Vectorial notation of the hypoplastic Cam-clay interface model

The definition proposed in Section 2.3 is used to derive the hypoplastic Cam-clay model (HCC) in a reduced notation. All the compoments of the model that have to be changed according to the newly defined operators are given in the following. The $\boldsymbol{L}$ matrix for the contact description is

$$\boldsymbol{L} = \begin{bmatrix} 1+\dfrac{\nu}{1-2\nu} & \dfrac{\nu}{1-2\nu} & 0 & 0 \\ \dfrac{\nu}{1-2\nu} & \dfrac{1}{2}\dfrac{\nu}{1-2\nu} & 0 & 0 \\ 0 & 0 & \dfrac{1}{2} & 0 \\ 0 & 0 & 0 & \dfrac{1}{2} \end{bmatrix} \tag{47}$$

where the stress invariant p is

$$p = -\frac{\sigma_t + 2\sigma_p}{3} \tag{48}$$

The deviatoric stress tensor can be written in vectorial notation:

$$\boldsymbol{\sigma}^* = \begin{bmatrix} \dfrac{2}{3}\sigma_t - \dfrac{2}{3}\sigma_p \\ \dfrac{\sigma_p}{3} - \dfrac{\sigma_t}{3} \\ \tau_x \\ \tau_y \end{bmatrix} \tag{49}$$

The invariant q is

$$q = \sqrt{\frac{3}{2}}\sqrt{\left(\frac{\sigma_t}{\sigma_t + 2\sigma_p} - \frac{1}{3}\right) + 2\left(\frac{\sigma_p}{\sigma_t + 2\sigma_p} - \frac{1}{3}\right) + 2\left(\frac{\tau_x}{\sigma_t + 2\sigma_p}\right) + 2\left(\frac{\tau_y}{\sigma_t + 2\sigma_p}\right)} \tag{50}$$

The asymptotic strain rate direction is

$$\boldsymbol{d} = \frac{3\begin{bmatrix} \frac{2}{3}\sigma_t - \frac{2}{3}\sigma_p \\ \frac{\sigma_p}{3} - \frac{\sigma_t}{3} \\ \tau_x \\ \tau_y \end{bmatrix} - \begin{bmatrix} 1 \\ 1 \\ 0 \\ 0 \end{bmatrix} p\frac{M^2 - \eta^2}{3}}{\|3\begin{bmatrix} \frac{2}{3}\sigma_t - \frac{2}{3}\sigma_p \\ \frac{\sigma_p}{3} - \frac{\sigma_t}{3} \\ \tau_x \\ \tau_y \end{bmatrix} - \begin{bmatrix} 1 \\ 1 \\ 0 \\ 0 \end{bmatrix} p\frac{M^2 - \eta^2}{3}\|} \tag{51}$$

For the definition of the hypoplastic Cam-clay interface model (see Eq. (3)) in vectorial notation, the term $\frac{\boldsymbol{\sigma}}{\lambda^*} \otimes \mathbf{1}$ is defined by

$$\frac{\boldsymbol{\sigma}}{\lambda^*} \otimes \mathbf{1} = \frac{\begin{bmatrix} \sigma_t & \sigma_t & 0 & 0 \\ \sigma_p & \sigma_p & 0 & 0 \\ \tau_x & \tau_x & 0 & 0 \\ \tau_y & \tau_y & 0 & 0 \end{bmatrix}}{\lambda^*} \tag{52}$$

The combination of all parts of the model then gives the hypoplastic Cam-clay model

as defined in (Eq. (21)):

$$\begin{bmatrix}\dot{\sigma}_t\\ \dot{\sigma}_p\\ \dot{\tau}_x\\ \dot{\tau}_y\end{bmatrix} = f_s\left(\begin{bmatrix}1+\frac{\nu}{1-2\nu} & \frac{\nu}{1-2\nu} & 0 & 0\\ \frac{\nu}{1-2\nu} & \frac{1}{2}\frac{\nu}{1-2\nu} & 0 & 0\\ 0 & 0 & \frac{1}{2} & 0\\ 0 & 0 & 0 & \frac{1}{2}\end{bmatrix} : \begin{bmatrix}\dot{\varepsilon}_t\\ 0\\ \frac{\dot{\gamma}_x}{2}\\ \frac{\dot{\gamma}_y}{2}\end{bmatrix}\right) +$$

$$f_s\left(-\frac{p}{p_e^*}\left(\frac{M^2+\eta^2}{M^2}\right) f_s\left(\begin{bmatrix}1+\frac{\nu}{1-2\nu} & \frac{\nu}{1-2\nu} & 0 & 0\\ \frac{\nu}{1-2\nu} & \frac{1}{2}\frac{\nu}{1-2\nu} & 0 & 0\\ 0 & 0 & \frac{1}{2} & 0\\ 0 & 0 & 0 & \frac{1}{2}\end{bmatrix} + \frac{\begin{bmatrix}\sigma_t & \sigma_t & 0 & 0\\ \sigma_p & \sigma_p & 0 & 0\\ \tau_x & \tau_x & 0 & 0\\ \tau_y & \tau_y & 0 & 0\end{bmatrix}}{\lambda^*}\right)\right)$$

$$\cdot f_s\left(\frac{3\begin{bmatrix}\frac{2}{3}\sigma_t - \frac{2}{3}\sigma_p\\ \frac{\sigma_p}{3} - \frac{\sigma_t}{3}\\ \tau_x\\ \tau_y\end{bmatrix} - \begin{bmatrix}1\\1\\0\\0\end{bmatrix} p\frac{M^2-\eta^2}{3}}{\|3\begin{bmatrix}\frac{2}{3}\sigma_t - \frac{2}{3}\sigma_p\\ \frac{\sigma_p}{3} - \frac{\sigma_t}{3}\\ \tau_x\\ \tau_y\end{bmatrix} - \begin{bmatrix}1\\1\\0\\0\end{bmatrix} p\frac{M^2-\eta^2}{3}\|}\|\dot{\boldsymbol{\varepsilon}}\|\right) \tag{53}$$

List of Tables

1. Parameters for the evaluation of HCC and HCE interface models 24
2. Parameters of the hypoplastic interface models used in the simulations . . 24
3. Properties of the different clays 24

Table 1: Parameters for the evaluation of HCC and HCE interface models

Parameters	Hypoplastic Cam-clay (**HCC**)	explicit Hypoplastic clay model (**HCE**)
λ^*	0.1	0.1
κ^*	0.01	0.01
ν	0.2	0.2
M/ϕ_c	0.98	25
N	1.0	1.0
κ_r	1.0	1.0

Table 2: Parameters of the hypoplastic interface models used in the simulations

Soils	λ^*	κ^*	ν	ϕ_c	N	κ_r
Illitic clay [4]	0.06	0.04	0.45	20	0.8	0.79
Kawasaki clay S0 (HCE) [2]	0.09	0.05	0.3	24	1.11	1.0 / 0.95 / 0.85
Kawasaki clay S0 (HCC) [2]	0.086	0.02	0.3	24	0.82	1.0 / 0.95 / 0.85
Kawasaki clay S4 (HCE) [2]	0.1	0.078	0.2	27	1.19	1.0
Kawasaki clay S4 (HCC) [2]	0.058	0.005	0.25	27	0.88	1.0
Kaolin clay [5]	0.11	0.02	0.2	22.5	1.03	0.75

Table 3: Properties of the different clays

Properties	Illitic clay [4]	Kawasaki clay [3]	Kaolin clay [5]
Plastic limit [%]	30.0	48.1	40.3
Liquid Limit [%]	83.0	86.0	75.3
Density ρ_s $[g/m^3]$	2.61	2.65	2.70

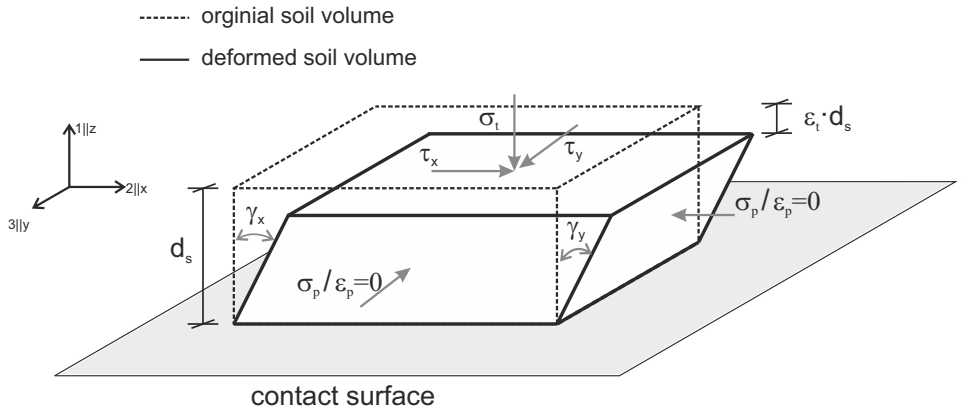

Figure 1: Definition of stresses and strains with additional local and global coordinate systems

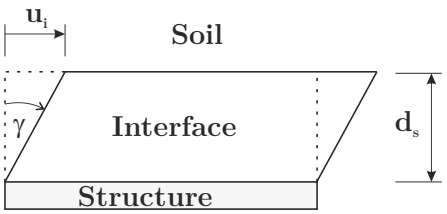

Figure 2: Schematic representation of the interface zone showing the relation between shear strain and shear deformation (modified from [28])

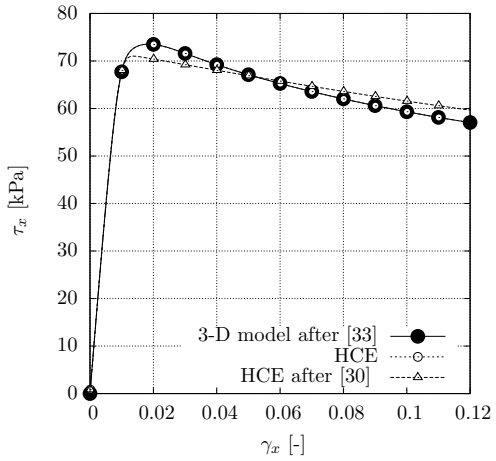

Figure 3: Comparison of 3-D continuum [33], interface constitutive model HCE and the interface constitutive model using the reduced tensor notation proposed by [30]

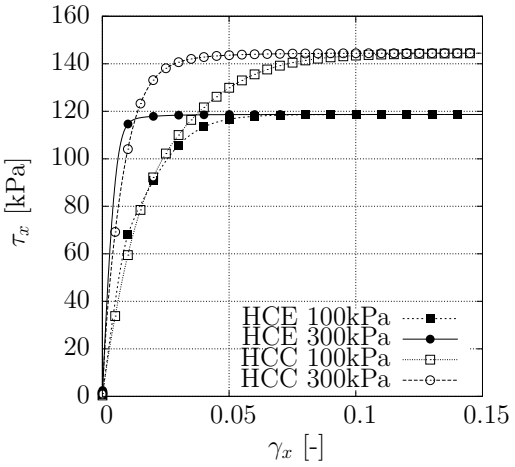

Figure 4: Stress path for constant volume boundary conditions: Shear stress τ_x vs shear strain γ_x for the Hypoplastic Cam-clay (HCC) and extended clay Hypoplastic (HCE) interface models for fine-grained soils

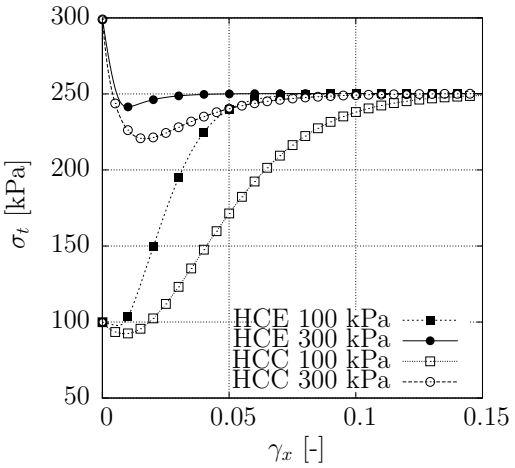

Figure 5: Stress path for constant volume boundary conditions: Normal stress σ_t vs shear strain γ_x for the Hypoplastic Cam-clay (HCC) and extended clay Hypoplastic (HCE) interface models for fine-grained soils

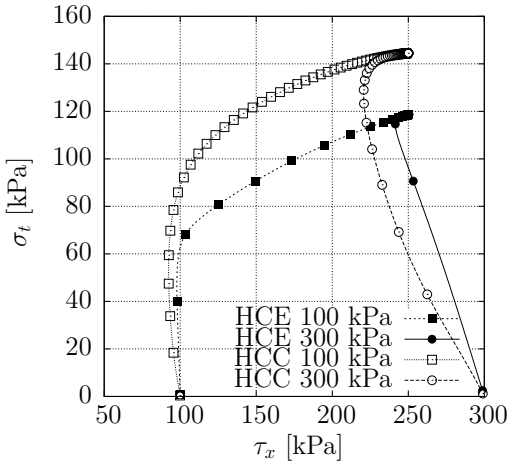

Figure 6: Stress path for constant volume boundary conditions: Shear stress τ_x vs normal stress σ_t for the Hypoplastic Cam-clay (HCC) and extended clay Hypoplastic (HCE) interface models for fine-grained soils

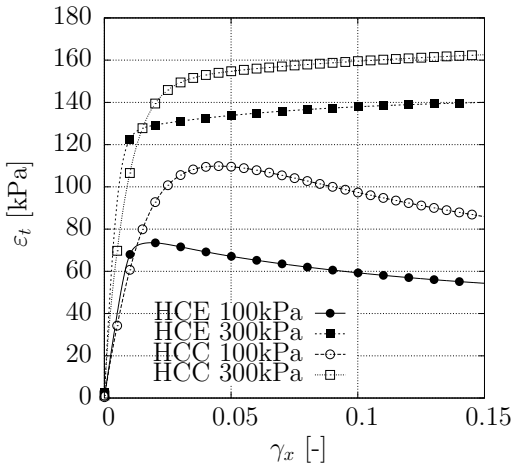

Figure 7: Constant normal stress conditions: Shear stress τ_x vs shear strain γ_x for the Hypoplastic Cam-clay (HCC) and extended clay Hypoplastic (HCE) interface models for fine-grained soils

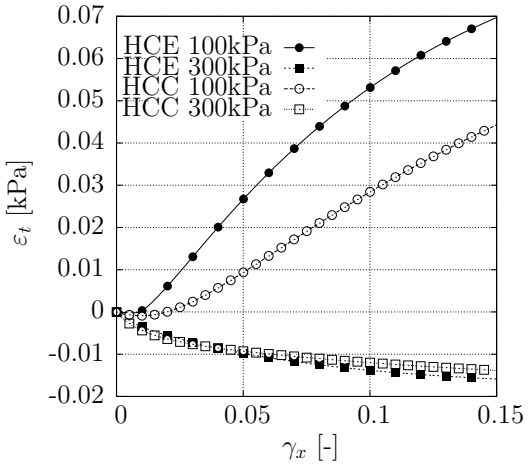

Figure 8: Constant normal stress conditions: Normal strain $\dot{\varepsilon}_t$ vs shear strain γ_x for the Hypoplastic Cam-clay (HCC) and extended clay Hypoplastic (HCE) interface models for fine-grained soils

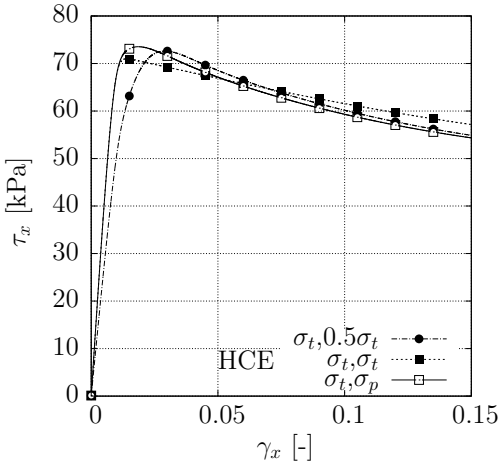

Figure 9: Constant normal stress conditions: Comparison of different applied initial stress conditions for the HCE model

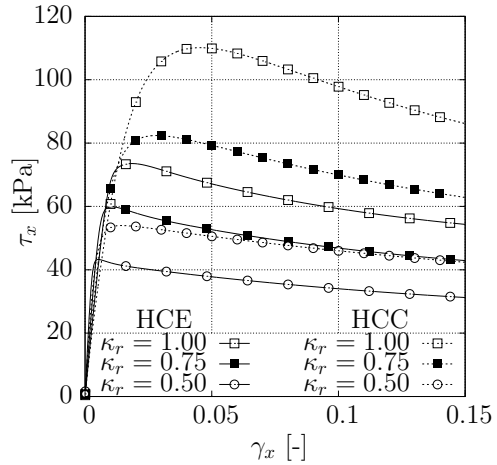

Figure 10: Comparison of constant normal Stress paths with varying roughness factors for the HCE and HCC interface models

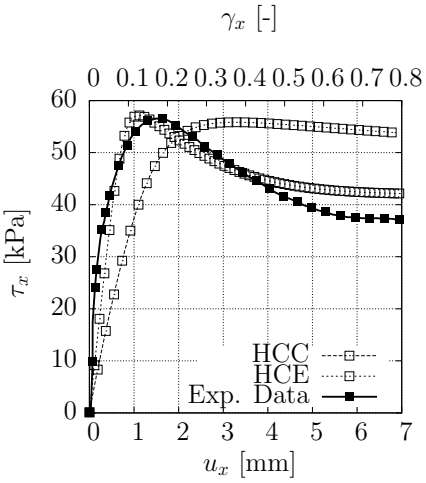

Figure 11: Verification using the experimental data of Littleton [4]

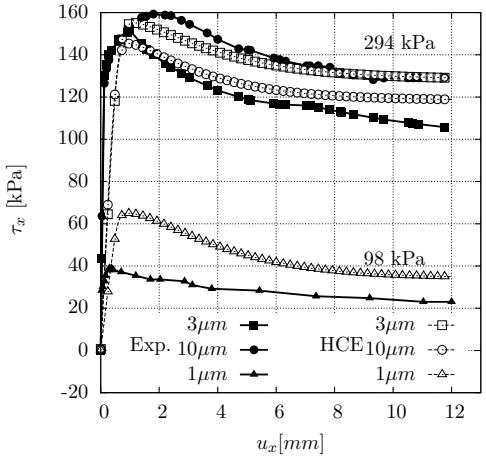

Figure 12: Verification for the HCE model using the experimental data of Tsubakihara et al. [2, 3] for Kawasaki marine clay (S0)

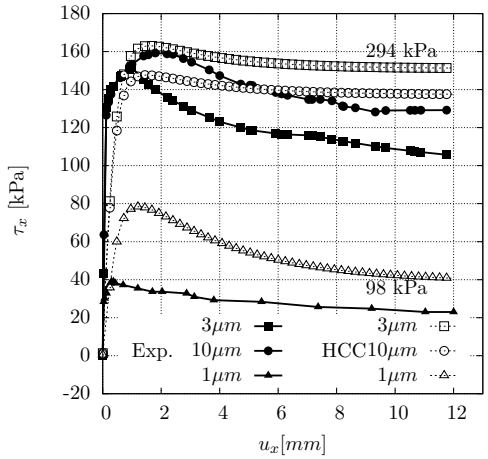

Figure 13: Verification for the HCC model using the experimental data of Tsubakihara et al. [2, 3] for Kawasaki marine clay (S0)

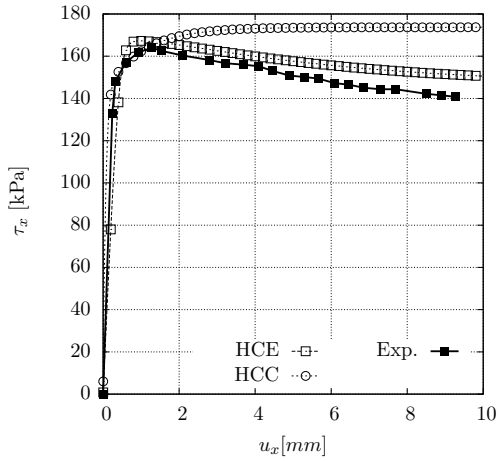

Figure 14: Verification using the experimental data of Tsubakihara et al. [2] for a mixture of Kawasaki marine clay with Toyoura sand (S4)

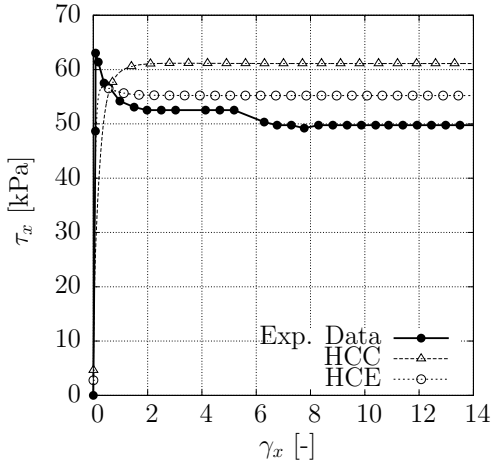

Figure 15: Verification using the experimental data of Sun et al. [5]